5th IAEA Technical Meeting on the Theory of Plasma Instabilities

# Current-interchange effect on tokamak stability and transport

L. J. Zheng* and W. Horton
Institute for Fusion Studies, University of Texas at Austin, Austin, TX 78712, USA
M. Furukawa
Graduate School of Frontier Sciences, The University of Tokyo, Kashiwa, Chiba, Japan
*E-mail: lzheng@mail.utexas.edu

**ABSTRACT**: We point out that interchange-type modes exchange not only thermal and magnetic energies between flux tubes, but also current. In a plasma with a current (or resistivity) gradient, such an interchange can create a current sheet at a mode resonance surface and result in the excitation of current-interchange tearing modes (CITMs). Instabilities of the interchange type could be directly converted into CITMs, alternative to forming turbulent eddies through nonlinear coupling as in conventional transport theories. This kink (or interchange) to tearing mode conversion offers another interpretation of enhanced electron transport in tokamaks. In particular, our CITM theory fills in the component in the Rechester and Rosenbluth transport theory [Phys. Rev. Lett. 40, 38 (1978)] for the origin of magnetic island structure in axisymmetric tokamaks.

# 1 Introduction

Instabilities of interchange type have been widely used to model anomalous transport in tokamaks in terms of the formation of turbulent eddies through nonlinear coupling. Rotation shear decorrelation of turbulence eddies is subsequently used to explain the formation of transport barriers. Experimental observations show that the electron energy transport is much larger than what one would expect from diffusive process due to Coulomb collisions. The electron Larmor radius is much smaller than ion one. Nonetheless, the electron thermal transport is stronger than ion one. This posts a challenge to tokamak transport theories. In Ref. [1], the broken magnetic surfaces due to the formation of magnetic island and stochastic field lines are proposed to explain the enhanced electron transport. But, how magnetic islands are formed in axisymmetric tokamak plasmas has not been given. The microtearing instabilities driven by electron temperature gradient are also proposed in this field for explaining the the formation of the magnetic islands [2] . However, this type of modes are usually stable in conventional tokamaks except near the plasma edge [2] . Our theory shows that interchange-type instabilities could be directly converted into current interchange tearing modes, instead of developing into the pure interchange nonlinear state. Note that electrons can move much faster than ions along the magnetic field lines. The current theory can help to clarify the cause of enhanced electron transport in tokamaks. In particular, our CITM theory fills in the component in the Rechester and

Rosenbluth transport theory [1] for the origin of magnetic island structure in axisymmetric tokamaks. Here we note that CITMs are not the rippling modes, since they have different parities [3].

## 2 On the rotation de-correlation effect

Due to unbalanced heating and so-called "intrinsic" rotation drives, tokamak plasmas rotate in general. Before we investigate CITMs, we first discuss the rotation de-correlation effect. The underlying physical picture for rotation de-correlation as commonly supposed is that the sheared flow carries the fluctuations on different magnetic surfaces with different speeds, so that the turbulence eddies are distorted and consequently the turbulent fluctuations on nearby surfaces are de-correlated.

We point out that this conventional physical picture about rotation de-correlation effect applies only to the case without magnetic shear. In the presence of magnetic shear the turbulence eddies are not de-correlated by rotation shear $d\Omega/d\psi$; instead, they are only de-correlated by rotation curvature $d^2\Omega/d\psi^2$.

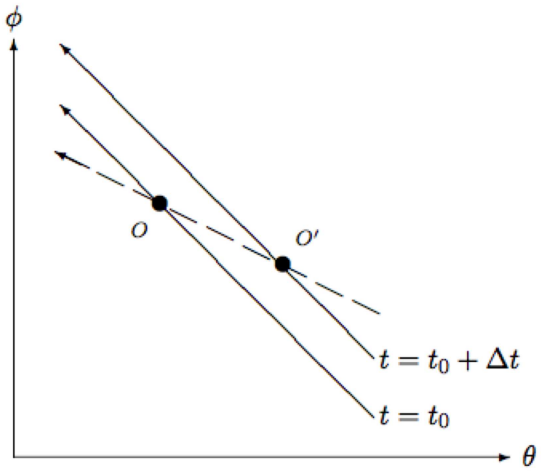


Figure 1: Two coordinates $\theta$ and $\phi$ indicate the poloidal and the toroidal directions, respectively. Dashed long arrow denotes the magnetic field line on the given magnetic surface. Two solid long arrows represent two magnetic field lines on the adjacent magnetic surface lying outwardly with respect to the given surface respectively at two time sequences: $t_0$ and $t_0+\Delta t$. The fixed correlation pattern of leading order is shown to propagate from point "$O$" to point "$O'$ " after a time interval $\Delta t$.

Let us use Fig. 1 to explain it. In Fig. 1, the dashed long arrow represents a magnetic field line on the given reference magnetic surface $\psi_0$, and two solid long arrows denote the magnetic field lines respectively at two time sequences $t_0$ and $t_0 + \Delta t$ on the adjacent magnetic surface $\psi_1$ which lies outwardly with respect to the reference surface $\psi_0$. The consideration is taken in the local frame moving together with the equilibrium velocity of dashed long arrow on surface $\psi_0$. The modes are supposed to locate around the point "$O$" initially at $t = t_0$. After a time interval $\Delta t$, the field line on the surface $\psi_1$ moves, relative to the dashed long arrow on the surface $\psi_0$ due to rotation shear. One can see that, as time evolves, the part of the mode lying on the left hand side of point "$O$" is de-correlated (or torn away as was referred to alternatively — i.e., the distance between dashed and solid lines, representing respectively two field lines on the two adjacent magnetic surfaces increases), while that on the right hand side tends to become instead more correlated

(pushed together — the distance between dashed and solid field lines tends to decrease). The flow shear acts as if pushing the fixed mode correlation pattern to propagate along the field: from point "$O$" at the time $t = t_0$ to point "$O'$" at the subsequent time $t = t_0 + \Delta t$. This shows that modes propagating along with local plasma rotation frames are not de-correlated by the rotation shear. Instead, the eddies just propagate along the filed line from "$O$" to "$O'$".

In the presence of rotation curvature, however, the relative "$O'$" points from each pair of two adjacent reference surfaces vary radially, and therefore modes are de-correlated by the rotation curvature.

# 3 Current interchange tearing modes

In this section we outline the CITM theory and underlying physics picture. The details can be found in Ref. [4]. We do not include the rotation effects into consideration explicitly. To fit our physical picture of CITMs onto the rotating plasma case, one just needs to consider the local frame moving from "$O$" to "$O'$" in Fig. 1. The rotation de-correlation discussed in the last section for turbulence eddies applies also to the magnetic island and field line chaotic structure. Also, in the following discussion we use Ohmic current as example. The theory can be extended to the case with non-Ohmic equilibrium currents, especially the bootstrap current.

## 3.1 Physics analysis

We first explain physical basis for the conversion of pressure-driven modes to current interchange tearing modes, *i. e.*, for the existence of CITMs. Figure 2 gives a schematic picture for this mode conversion process. We consider a rational surface (dot-dashed line). The minor radius points up, and therefore the gradient of the plasma electric conductivity $\nabla\sigma$ (or generally current gradient) points down. Both the magnetic field and the Ohmic current at the rational surface are directed out of the plane of Figure 2. The equilibrium magnetic field in the orthogonal direction with respect to the magnetic field on the rational surface, $\boldsymbol{B}_*$, is denoted by horizontal arrows. Boldface is used to denote vectors. $\boldsymbol{B}_*$ switches its direction across the rational surface. If the system is unstable to pressure-driven modes, a radial plasma displacement $\xi_r$ of the interchange type (solid curve) develops. In the conventional physical picture for

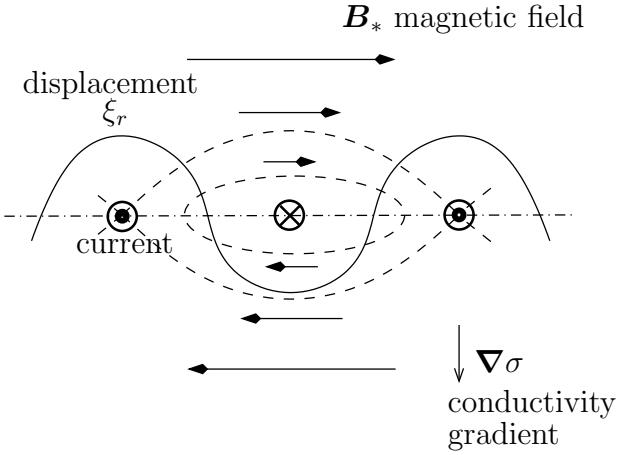


Figure 2: CITM physics picture

the Rayleigh-Taylor instability, these perturbations develop when the total thermal and magnetic energy is reduced. Because the electric conductivity in tokamaks is generally inhomogeneous, the equilibrium current profile is not flat in the radial direction. Consequently, interchange-type perturbations carry not only plasma and magnetic energies, but also current, by carrying along plasma temperature. This creates alternating hills and holes of plasma current at the rational surface. Where plasma balloons out from the core, a current hill is created (denoted in Fig. 2 by circled dots). Instead, Where plasma shrinks to the core, a current hole is created, which is equivalent to a perturbed current being formed that is opposite to the equilibrium current at the rational surface. In Fig. 2, a current hole is denoted by a circled "×". A current hill induces a counter-clockwise magnetic field, whereas a current hole gives rise to a clockwise magnetic field. When these perturbed magnetic fields are added to the equilibrium magnetic field $\boldsymbol{B}_*$, the result is a magnetic island chain, denoted by the dashed curves in Fig. 2. This explains the mode conversion process from pressure-driven to current-driven tearing modes in tokamak plasmas.

## 3.2 Linear theory

In this subsection we demonstrate the existence of CITMs in the linear theory framework. We consider high $n$ or radially localized modes, where $n$ is the toroidal mode number. The time ($t$) dependence is assumed to be $\exp\{\gamma t\}$, where $\gamma$ is the growth rate. The basic set of equations is derived from the equation of motion (or the so called vorticity equation) and magnetic diffusion equation. With the stream functions ($\boldsymbol{\xi}_\perp \propto \boldsymbol{b}\times\boldsymbol{\nabla}\delta\varphi$ and $\delta\boldsymbol{B}_\perp \propto \boldsymbol{b}\times\boldsymbol{\nabla}\delta\psi$) and ballooning representation introduced, the following two coupled equations can be obtained:

$$\frac{\partial}{\partial\theta}\left(\frac{\dot\chi^3}{B^2}\boldsymbol{C}^2\delta\psi\right)+2\dot p(\kappa_v+\kappa_\zeta\dot q\theta)\delta\varphi-\rho\gamma^2\frac{\dot\chi^2}{B^2}\boldsymbol{C}^2\delta\varphi=0, \tag{1}$$

$$\left[1+(n^2\eta/\gamma)\boldsymbol{C}^2\right]\delta\psi=\dot\chi\frac{d\delta\varphi}{d\theta}+i\frac{\Sigma'}{\gamma}\delta\varphi, \tag{2}$$

where $\boldsymbol{C}^2=(\boldsymbol{\nabla}\zeta-\dot q\theta\boldsymbol{\nabla}v)^2$, $\Sigma'=(1/\dot\chi)nqE_\phi(d\ln\sigma/dv)$, $E_\phi$ is toroidal equilibrium electric field, $\boldsymbol{b}=\boldsymbol{B}/B$, $\boldsymbol{\kappa}=\boldsymbol{b}\cdot\boldsymbol{\nabla}\boldsymbol{b}$ is the magnetic field line curvature, with $\kappa_v$ and $\kappa_\zeta$ being its normal and geodesic components, $\sigma$ is the electric conductivity, and dot denotes derivative with respect to volume $v$. Equations (1) and (2) can be combined to give the follwing equation:

$$\frac{\partial}{\partial\theta}\left[\frac{1}{B^2}\frac{\boldsymbol{C}^2}{1+(n^2\eta/\gamma)\boldsymbol{C}^2}\left(\frac{\partial}{\partial\theta}\delta\varphi+i\frac{\Sigma'}{\gamma}\delta\varphi\right)\right]+\frac{2\dot p}{\dot\chi^4}(\kappa_v+\dot q\theta\kappa_\zeta)\delta\varphi-\rho\gamma^2\frac{1}{\dot\chi^2B^2}\boldsymbol{C}^2\delta\varphi \;=\; 0. \tag{3}$$

Note that inclusion of resistivity gradient $\Sigma'$ breaks the symmetry of the mode about rational surface.

To get a basic picture for the conversion from resistive interchange modes to CITMs, we first investigate the resistivity gradient effect on resistive interchange modes in the

cylinder limit [5, 6]. In this case, it is assumed that $(\eta/\gamma)\boldsymbol{C}^2 \gg 1$. With cylindrical symmetry, the geodesic curvature $\kappa_\zeta = 0$ vanishes and the equilibrium quantities become independent of $\theta$. Therefore, equation (3) reduces to

$$\frac{\partial^2 \delta\varphi}{\partial\theta^2} + i\frac{\bar{\Sigma}'}{\gamma}\frac{\partial \delta\varphi}{\partial\theta} + \left(ns\sqrt{\gamma\eta}\Lambda - \gamma\eta n^2 s^2\theta^2\right)\delta\varphi \;\; = \;\; 0, \tag{4}$$

where $\Lambda = 2n\dot{p}\kappa_v|1/\dot{q}|\boldsymbol{\nabla} v|\dot{\chi}^3|(\eta/\rho\gamma^3)^{1/2}$ and $\bar{\Sigma}' = \Sigma'|\dot{\chi}/n\dot{q}|\boldsymbol{\nabla} v||(\eta/\rho\gamma^3)^{1/2}$. The second term in this equation is due to the resistivity gradient effect.

Equation (4) can be reduced to Kummer's eqution [7]

$$z\frac{d^2\delta u}{dz^2} + \left(\frac{3}{2} - z\right)\frac{d\delta u}{dz} - \left(\frac{3}{4}\frac{\bar{\Sigma}'^2/\gamma^2 + 4ns\sqrt{\gamma\eta}\Lambda}{16ns\sqrt{\gamma\eta}}\right)\delta u = 0, \tag{5}$$

by the following two consecutive transforms $\delta\varphi = \theta^{-1/2}e^{-i\frac{1}{2}(\bar{\Sigma}'/\gamma)\theta}\delta F$, $\delta F = z^{\frac{3}{4}}e^{-\frac{1}{2}z}\delta u(z)$, where, $z = ns\sqrt{\gamma_N\eta}\theta$. Kummer's equation, Eq. (5), can be solved analytically. The eigen function is

$$\delta\varphi \;\; = \;\; (n^2s^2\gamma\eta)^{\frac{1}{8}}2^{-k}e^{-i\frac{\bar{\Sigma}'}{2\gamma}\theta - \frac{1}{2}ns\sqrt{\gamma\eta}\theta^2}H_k((n^2s^2\gamma\eta)^{1/4}\theta) \tag{6}$$

and the eigen value is determined by the following dispersion relation

$$\frac{\bar{\Sigma}'^2/\gamma^2 + 4ns\sqrt{\gamma\eta}\Lambda}{4ns\sqrt{\gamma\eta}} = 2k + 1, \tag{7}$$

where, $k = 0, 1, 2, \cdots$ and $H_k$ is the Hermite polynomial. The radial magnetic field $\delta\psi$ can be obtained by inserting $\delta\varphi$ in Eq. (6) into Eq. (2).

Without the resistivity gradient effect (*i.e.*, $\bar{\Sigma}' = 0$), the dispersion relation in Eq. (7) reduces to the resistive interchange stability condition in Refs. [5] and [6]: $\dot{p}\kappa_v < 0$, which is more stringent than the Suydam criterion [8] . The dispersion relation in Eq. (7) shows the resistivity gradient effect on the growth rate. For tokamaks with the loop voltage being a few volts and the equilibrium magnetic field several Teslas, the dimensionless parameter $\bar{\Sigma}'$ is of order $10^{-5} - 10^{-4}$ as compared to the Alfvén frequency $\Omega_A$. Using this estimate, one can see that, for $\gamma/\Omega_A \sim 10^{-3}$, the $\bar{\Sigma}'$ effect on growth rate is not dramatic. However, the $\bar{\Sigma}'$ effect on the conversion from resistive interchange modes to CITMs is significant. This can be seen from the eigen function in Eq. (6). Without the resistivity gradient effect, the eigen function is symmetric with respect to $\theta$. Using Eq. (2), one can see that the perturbed radial magnetic field $\psi$ is odd in this case. Therefore, the perturbed radial magnetic field vanishes at the rational surface and no field line reconnection can occur. In the presence of the resistivity gradient effect (*i.e.*, $\bar{\Sigma}' \neq 0$), the eigen function $\delta\varphi$ becomes complex and non-symmetric and consequently an even (*i. e.*, tearing mode parity) component of the perturbed radial magnetic field appears. This is due to the factor $\exp\{-i\bar{\Sigma}'\theta/(2\gamma)\}$ in the eigen function in Eq. (6). Because the resistive modes are localized in the configuration space, they extend broadly along the ballooning mode space. The coordinate $\theta$ can be a few tens to hundred. This makes this factor to be finite. This factor breaks the resistive interchange mode symmetry and gives rise to the tearing parity

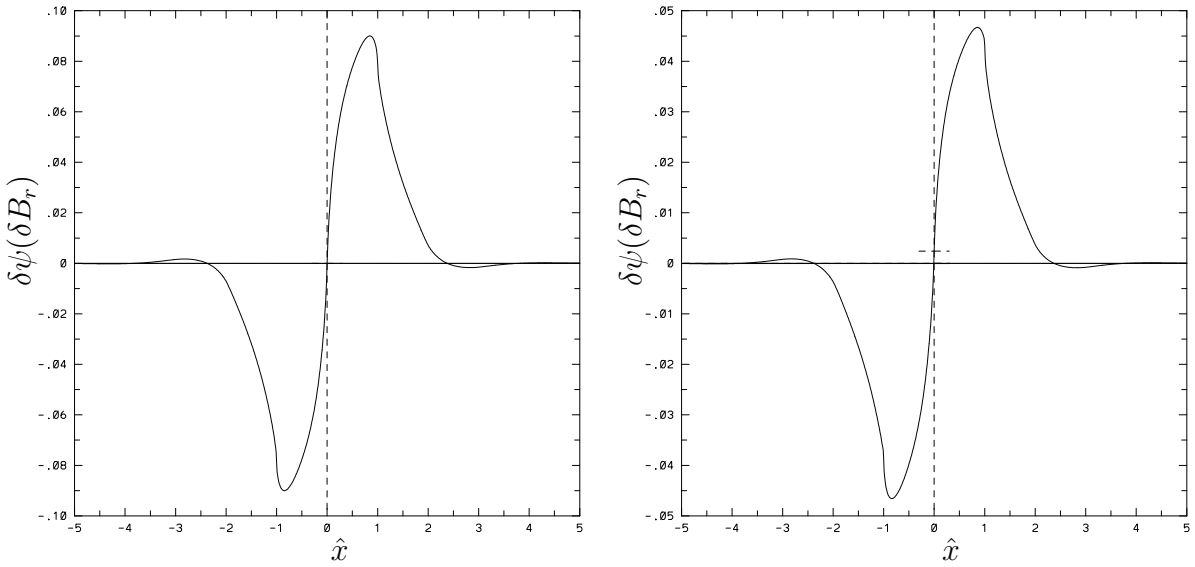


Figure 3: Mode conversion from resistive ballooning (left) to tearing (right) modes

modes. As well-known, a non-vanishing radial magnetic field at the rational surface can cause the field line reconnection. This shows the conversion from resistive interchange modes to CITMs. This also shows that CITMs are different from the so-called rippling modes [3], which also results from resistivity gradient.

It is also interesting to examine how the pressure driven modes are converted to CITMs in the toroidal geometry. The ballooning representation is used to account for toroidal coupling. We employ the $s-\alpha$ equilibrium model [9]. In this equilibrium, the resistive ballooning mode equation becomes

$$\frac{\partial}{\partial\theta}\left[\frac{\bar{\boldsymbol{C}}^2}{1+(\eta^*/\gamma_N)\bar{\boldsymbol{C}}^2}\left(\frac{\partial}{\partial\theta}\Phi+i\frac{\Sigma'^*}{\gamma_N}\delta\varphi\right)\right]+\alpha\{\cos\theta+f(\theta)\sin\theta\}\delta\varphi-\gamma_N^2\bar{\boldsymbol{C}}^2\delta\varphi \;=\; 0, \quad (8)$$

where $\eta^*=n^2\eta/(R^2\Omega_A)$, $\Sigma'^*=\bar{\Sigma}'/\Omega_A$, $\bar{\boldsymbol{C}}^2=1+f^2(\theta)$, and $f(\theta)=s\theta-\alpha\sin\theta$. We solve Eq. (8) numerically using AEGIS-1D (Adaptive EiGenfunction Independent Solution - 1 Dimension) code. AEGIS-1D code is a linear adaptive shooting code in the ballooning representation space, supplementary to 2D AEGIS code [10] for high-n ballooning calculation. The same numerical scheme as 2D AEGIS is used in AEGIS-1D code. Figure 3 shows the solutions of Eq. (8) without (left) and with (right) resistivity gradient taken into account. The figure is plotted in real space $x$ by performing the inverse ballooning transform. Noting that $\Delta'=0$ in the $s-\alpha$ equilibrium model, the classical tearing modes are non-existant in this case. Therefore, without resistivity gradient taken into account the radial magnetic field $\delta\psi$ vanishes at the rational surface $x=0$, as shown in the left part of Fig. 3. When the resistivity gradient is introduced, the radial magnetic field $\delta\psi$ becomes finite at the rational surface $x=0$, as shown in the right part of Fig. 3. This demonstrates the conversion from restive ballooning modes to CITMs due to the inclusion of current gradient.

### 3.3 Nonlinear theory

In this section, we analyze this mode conversion process nonlinearly. We employ the conventional approach based on the Rutherford equation [11] to show how a current sheet can develop and magnetic islands are formed, as the pressure-driven modes become unstable. The basic set of equations describing interchange type of modes and tearing modes are given by the vorticity and magnetic diffusion equations:

$$i\frac{R}{nB_\phi}sx\frac{d^2\delta B_r}{dx^2}+\frac{\gamma^2}{n^2\omega_A^2}\frac{d^2\xi_r}{dx^2}-\left(\frac{1}{4}-D\right)\xi_r=0, \tag{9}$$

$$\frac{\partial^2\delta B_r}{\partial x^2}=\tau_r\frac{\partial\delta B_r}{\partial t}+i\frac{n\tau_r Bs}{R}x\frac{\partial\xi_r}{\partial t}+i\frac{m\tau_r J_\phi}{\sigma r_s^2}\frac{d\ln\sigma}{dx}\xi_r, \tag{10}$$

where $\delta B_r$ is the perturbed radial magnetic field, $\tau_r=\sigma r_s^2$ is the resistive time, $r_s$ is the minor radius at the rational surface, $R$ is the major radius, and $D$ is the so-called Mercier index. The last term in Eq. (10) is the term describing the current interchange effect.

Equations (9) and (10) have two types of solutions: tearing-type modes, which have even parity for $\delta B_r$ at the rational surface, and pressure-driven modes, which have odd parity [12]. Here we consider the even parity (*i.e.*, tearing) modes. The last two terms in Eq. (10) represent the coupling of pressure-driven modes. As shown in Ref. [11], the second term on the right-hand side of Eq. (10) can be removed by a suitable surface average. Then, following the procedure used to derive the classical Rutherford equation in Ref. [11], one can extend the linear tearing mode equation (10) into the nonlinear version:

$$\tau_r\frac{\partial w}{\partial t}=\frac{\sqrt{Rr_s}}{\sqrt{2}A}\Delta'+\hat{\Sigma}'\sqrt{Rr_s}\frac{\xi_r(r_s)}{w}, \tag{11}$$

where $w=4\sqrt{(Rr_s/ns)(\delta B_r/B)}$ is the width of the magnetic island, $\Delta'=(d\delta B_r/dx)/\delta B_r|_{r_s^-}^{r_s^+}$, $\hat{\Sigma}'=(8qJ_\phi/B_\phi s^{3/2}\sigma)|d\ln\sigma/dr|\tau_r$ describes the coupling of pressure-driven modes, and $A\approx 0.7$ as given in Ref. [11]. From Eq. (11) one can derive a new stability criterion for tearing modes:

$$\Delta'+\hat{\Sigma}'\sqrt{2}A\frac{\xi_r(r_s)}{w}<0. \tag{12}$$

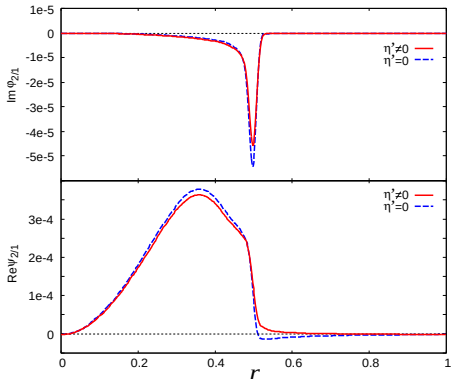


Figure 4: Mode conversion

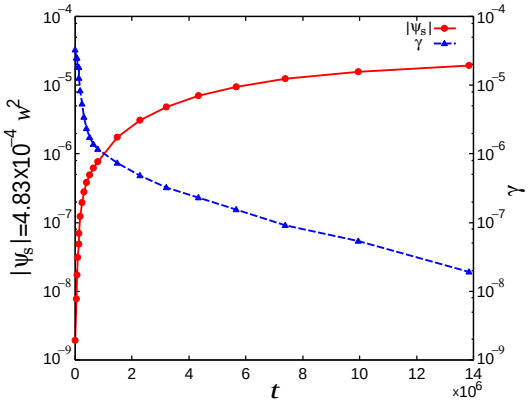


Figure 5: Quasilinear growth rate $\gamma$ and island width $w$ ($\psi_s$) saturation with time $t$.

This new criterion differs from the classical tearing mode stability criterion $\Delta' < 0$ by having an additional driving term resulting from current gradient effect. Note that anomalous transport is usually related to high $n$ modes. While for high-n mode $\Delta'$ is small due to the ballooning translational invariance and therefore the current gradient effect is significant. Furthermore, the second term in Eq. (12) is inversely proportional to the island width. This makes the current interchange effect can play a dramatic role in converting interchange type of modes to tearing modes in the initial stage of mode development.

A numerical example of this type of mode conversion is shown with the viscous fluid model in slab geometry. Figure 4 shows the linear eigenmode as a function of minor radius for the cases with (solid curve) and without (dashed curve) resistivity gradient effect. Without resistivity gradient effect taken into account, the mode is a pure resistive interchange mode (with computed $\Delta' = -4.15$), for which the radial magnetic perturbation $\psi$ at the rational surface is negligible. The linear growth rate normalized to the Alfvén frequency is $3.2 \times 10^{-5}$. When the resistivity gradient effect is taken into account, however, the radial magnetic perturbation $\psi$ at the rational surface becomes finite. Consequently, a mode of tearing parity appears, with growth rate $4.1 \times 10^{-5}$. This confirms the conversion of pressure-driven modes to current-interchange tearing modes. Figure 5 shows the quasilinear evolutions of radial magnetic field (or, equivalently, the island width $w$) and quasilinear growth rate.

# 4 Conclusions and discussion

In conclusion, we show that unstable electromagnetic and electrostatic modes of the interchange type (*e.g.*, interchange/ballooning modes, drift waves, *etc.*) can convert to tearing modes. This gives another explanation for enhanced electron transport observed in tokamak experiements. Note that current gradient effect can become especially significant for high $n$ modes due to smallness of $\Delta'$. Since high-n modes are regarded as the main cause for anomalous transport, inclusion of current interchange effect in the anomalous transport interpretation and simulation becomes necessary. For example, the well-known unstable ballooning modes between the 1st and 2nd stability regimes in the $s - \alpha$ equilibrium model [9] become actually unstable tearing modes.

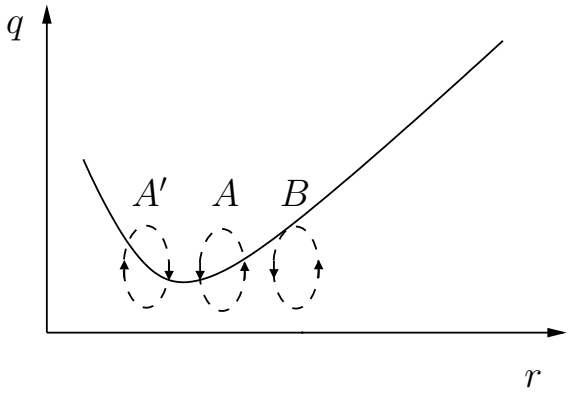

Figure 6: Transport barrier picture.

It is also interesting to discuss the transport barrier phenomenon. The reduced particle transport at reversed shear region has been reported in the simulations based on the theories of broken magnetic surfaces [13, 14]. The conversion from the interchange-type

of modes to CITMs gives a support to the transport barrier theory based on the broken magnetic surfaces. An intuitive picture for transport barrier is given as follows. As shown in Fig. 6, the island (including the associated stochastic field) rotational transform reverses direction across a $q$ minimum. As islands grow and reconnect in the case without magnetic shear reversal (islands "$A$" and "$B$" and their associated stochastic field), magnetic energy can be released and the radial transport step size increased. However, this type of island-island reconnection is restricted at safety factor extremes (islands "$A$" and "$A'$" and their associated stochastic field). Enhanced transport due to island-island and their associated stochastic field reconnection in the normal shear case has been reported in the reversed field pinch experiments [15]. The reconnection forbidden layers are observed at the $q$ maximum in the reversed field pinch experiments [16] . These layers are termed as the so-called ghost surfaces. Ghost surfaces were originally introduced for the standard map to denote surfaces which are nonintersecting (in this context, they are called ghost circles) [17, 18]. We point out here that at $q$ extremes such type of ghost surfaces can be formed naturally due to different wiring directions of island (and their associated stochastic region) field lines on the opposite sides of $q$ extreme. It is interesting to point out that, based on the analysis in Sec. 2, the rotation shear de-correlation also occurs only at the safety factor extremes. This coincidence seems to double support the correlation between transport barriers and safety factor extremes.

# References


[1] A. B. Rechester and M. N. Rosenbluth, Phys. Rev. Lett. **40**, 38 (1978).
[2] J. W. Connor, S. C. Cowley, and R. J. Hastie, Plasma Phys. Control. Fusion **32**, 799 (1990).
[3] H. P. Furth, J. Killeen, and M. N. Rosenbluth, Phys. Fluids **6**, 4826 (1963).
[4] L. J. Zheng and M. Furukawa, Phys. Plasmas **17**, 052508 (2010).
[5] J. L. Johnson and J. M. Greene, Plasma Phys. **9**, 611 (1967).
[6] D. Correa-Restrepo, Z. Naturforsch. **37a**, 848 (1982).
[7] M. Abramowitz and I. A. Stegun, Handbook of Mathematical Functions (Dover Publications, Inc., New York, 1972) 503.
[8] B. R. Suydam, in Proc. 2nd UN international Conf. PUAE, United Nations, Geneva, **31**, 157 (1958).
[9] J. W. Connor, R. J. Hastie, and J. B. Taylor, Phys. Rev. Lett. **40**, 4396 (1978).
[10] L.-J. Zheng and M. Kotschenreuther, J. Comp. Phys. **211**, 748 (2006).
[11] P. H. Rutherford, Phys. Fluids **16**, 1903 (1973).
[12] A. H. Glasser, J. M. Greene and J. L. Johnson, Phys of Fluids. **18**, 875 (1975).
[13] D. del-Castillo-Negrete and P. J. Morrison, Phys. Fluids **A5**, 948 (1993).
[14] P. J. Morrison and A. Wurm, Scholarpedia, **4**, 3551 (2009).
[15] J. S. Sarff, Bull. Am. Phys. Sci. **54**, 178 (2009).
[16] M. E. Puiatti et al., Plasma Phys. Control. Fusion **51**, 124031 (2009).
[17] C. Golé, J. Diff. Equ. **97**, 140 (1992).
[18] R. S. MacKay and M. R. Muldoon, Phys. Lett. **A 178**, 245 (1993).